EFFECTS ON THE DYNAMIC BEHAVIOUR OF ROTORS ON AMB OF THE ELECTROMECHANICAL COUPLING IN INDUCTION MOTORS

Nicola Amati and Eugenio Brusa
Department of Mechanics, Politecnico di Torino, Torino, Italy,
amati@polito.it, brusa@polito.it
Giuseppe Gianolio
Department of Electric Engineering, Politecnico di Torino, Torino, Italy,
gianolio@athena.polito.it

ABSTRACT

The role of the unbalanced magnetic pull exerted by the magnetic field of induction motors on rotors supported by active magnetic bearings is investigated at least in the range of spin speeds corresponding to the rigid body behaviour. Under the assumptions that the forces of the bearings can be linearized and the rotor is axially symmetrical, the equations of motion of the system are written including the negative stiffness of the motor due to non uniform air gap. Some numerical results are then compared to the experimental data performed on a spindle on magnetic suspension, with five active axes. The effects at different values of the spin speed and in presence of slip in the induction motor are then analysed with particular care to the vibration condition monitoring of the whole machine.

INTRODUCTION

Unbalanced magnetic pull (u.m.p.) can occur in electric machines when a lack of axial symmetry of the air gap occurs. In the case of rotors on ball and roller bearings this unbalance is usually due to permanent or elastic deformations of the rotor and of the stator, while in the case of active magnetic suspension, it can be detected also in presence of rigid body motion of the rotor. The u.m.p. affects the flexural dynamic behaviour of the system, by introducing an additional negative stiffness. In case of static eccentricity this force is exerted towards the minimum air gap, while in dynamic conditions its amplitude and frequency depend on the spin speed of the rotor and on the slip speed of the motor. In vibration condition monitoring the radial displacements measured by the position sensors suffer a relevant change in amplitude, also at constant spin speed, because of the beat occurring between the u.m.p. and the unbalance forces of the rotor. This phenomenon is particulary evident at lower values of the spin speed. A suitable model for the analysis of the effects caused by the u.m.p. on the dynamic behaviour of the rotor on AMBs is proposed. The negative stiffness due to the induction motor is computed according to some methods present in literature based on the analysis of the magnetic flux density within the air gap mainly in case of the static eccentricity of the rotor ([1], [2], [3], [4], [5], [6]). The equations of motion of a rotor on active magnetic suspension powered by a induction motor are written in the case of dynamic eccentricity. The interaction between the u.m.p. and the slip speed of the induction motor is taken into account in the model. Experimental results, based on the radial displacements measured on a spindle on AMBs with five active axes [7], with a mass of about 6 kg and equipped with a two poles induction motor, are then compared to the numerical predictions performed by the proposed model.

INDUCTION MOTOR MODEL

Several analytical, FEM and FDM methods ([1], [2], [3], [4], [5]) have been proposed to predict the flux density distribution and the u.m.p. in induction machines with non uniform air gap. A simple analytical approach of a two poles electric motor [5] predicts the u.m.p. caused by static eccentricity. End effects, effects of slotting, saturation, eddy currents, variations in magnetic permeability are neglected in the first approximation of the mentioned model. The u.m.p. is here modelled according to [5] and then accounted for in the dynamic model of the controlled rotor on

AMBs.

A polar reference frame can be assumed for the description of the static non uniform air gap, with the x axis directed towards the minimum air gap and the angular coordinate ϑ being in the counter-clockwise direction [5]. If $\epsilon/R \ll 1$, where ϵ and R are respectively the eccentricity and the radius of the rotor, the air gap h can be expressed as:

$$h = c\,(1 + \epsilon^* \cos\vartheta) \tag{1}$$

where the nondimensional eccentricity $\epsilon^* = \epsilon/c$, (c is the uniform air gap) can be computed in terms of the nondimensional coordinates of the center of the rotor $x^* = x/c$, $y^* = y/c$ as:

$$\epsilon^* = \left(\sqrt{x^{*2} + y^{*2}}\right). \tag{2}$$

According to the approach described in [5], the air gap m.m.f. can be written as:

$$M = M_0[\cos(\vartheta - \omega_m t) + \frac{1}{2}\epsilon^* \cos\omega_m t] \tag{3}$$

where the first term is the fundamental m.m.f. harmonic component, while the second one takes into account the contribution due to the variation in time of the magnetic potential caused by the rotor eccentricity. This term is accounted for to avoid a violation of the Gauss theorem in the case of a two-dimensional solution for the magnetic flux density [5]. M_0 is the peak value of ampere turns per pole and is computed as $M_0 = 3NI_mK_{pd}/\pi$ (symbols are: N the series turns per phase in the stator winding, K_{pd} the stator winding factor, I_m the peak fundamental magnetizing current), while ω_m is the angular velocity of the rotating magnetic field.

If $\epsilon^* \ll 1$, the air gap magnetic flux density components are:

$$B_r = B_{r1}\cos(\vartheta - \omega_m t) - B_{r2}\cos(2\vartheta - \omega_m t) \tag{4}$$

$$B_\vartheta = 0. \tag{5}$$

while B_{r1} and B_{r2} are given by:

$$B_{r1} = \frac{\mu_0 M_0}{c};\; B_{r2} = \frac{1}{2}\epsilon^* B_{r1}. \tag{6}$$

According to equation (5) the rotor eccentricity causes a four-pole component in the magnetic field, which rotates at half speed. Actually if the model is based on the current sheet computation in the rotor, according to Swann (reported in [5]) the same approach states that a more suitable value for the ratio (6) is:

$$B_{r2} = \frac{1}{4}\epsilon^* B_{r1}. \tag{7}$$

The eddy currents generated by the magnetic field and their influence on the reduction of the u.m.p. have been also investigated by Stoll [5] in a second approximation model, but are here neglected. The components of the force due to the magnetic field expressed in equation (5) are:

$$F_x = \int_0^{2\pi} (\sigma_r \cos\vartheta - \sigma_\vartheta \sin\vartheta)\, R d\vartheta = -F \tag{8}$$

$$F_y = \int_0^{2\pi} (\sigma_r \sin\vartheta - \sigma_\vartheta \cos\vartheta)\, R d\vartheta = 0 \tag{9}$$

$$F = \frac{B_{r1}B_{r2}\pi R}{2\mu_0} \tag{10}$$

where σ_r and σ_ϑ are the radial and circumferential Maxwell stresses [8]. From equation (10) the amplitude of the negative stiffness due to the u.m.p. can be computed as:

$$|k_m| = \frac{\mu_0 \pi R M_0^2 l_m}{4c^3} \tag{11}$$

where l_m is the axial length of the motor, and the direction of the force is towards the minimum air gap in case of static eccentricity and no slip.

MODEL OF ROTOR ON AMB WITH U.M.P. EFFECT

A quite classical approach for the analysis of the dynamic behaviour of a four degrees of freedom model of axially symmetrical rotors on AMB is based on the complex displacement and rotation of the rotor at the center of gravity [9]. Since the rotor, which is used for the experimental validation, is supported by two radial AMBs and noncolocated position sensors measure the radial displacements along the directions of the forces exerted by the actuators, equations of motion are here written assuming as degrees of freedom the displacements monitored by the sensors $\mathbf{x}_s = [x_{1s}\; y_{1s}\; x_{2s}\; y_{2s}]^T$ [10]:

$$\mathbf{M}^*\ddot{\mathbf{x}}_s + \hat{\mathbf{C}}^*\dot{\mathbf{x}}_s + \hat{\mathbf{K}}^*\mathbf{x}_s = \mathbf{T}_s^T(\omega^2\mathbf{f}_r e^{j\omega t} + \mathbf{f}_m e^{j\omega_s t}) \tag{12}$$

where $\hat{\mathbf{C}}^* = \mathbf{C}^* - \omega\mathbf{G}^*$ and $\hat{\mathbf{K}}^* = \mathbf{K}^* - \mathbf{K}_\mathbf{u}^*$. Equation (12) is written in an inertial reference frame. Matrices $\mathbf{M}^*$, $\mathbf{C}^*$, $\mathbf{G}^*$, $\mathbf{K}^*$, $\mathbf{K}_\mathbf{u}^*$, $\mathbf{T}_s^T$, are reported in [10]. $\mathbf{M}^*$ and $\mathbf{G}^*$ are the mass and gyroscopic matrices, $\mathbf{C}^*$, $\mathbf{K}^*$, $\mathbf{K}_\mathbf{u}^*$ are the damping and stiffness matrices due to the controlled magnetic bearings under the assumption that the actuator forces can be linearized [9]. Assuming that the rotor behaves as rigid body, the transformation matrix $\mathbf{T}_s^T$ allows the transition from the degrees of freedom of the center of gravity to the displacements at the sensors location. Vectors $\mathbf{f}_r$ and $\mathbf{f}_m$ include the rotor unbalance forces and the u.m.p. of the motor, while ω and ω_s are respectively

the angular velocity of the shaft and of the u.m.p. In presence of slip speed in the induction motor the amplitude of the negative stiffness k_m, added by the u.m.p., looks constant in the non inertial reference frame rotating at the spin speed:

$$\omega_s = \frac{\omega + \omega_m}{2} \tag{13}$$

i.e. in the rotating reference frame of the magnetic field the same stiffness oscillates with a frequency which corresponds to the angular velocity:

$$\omega_{pull} = \frac{\omega - \omega_m}{2}. \tag{14}$$

To introduce the u.m.p. stiffness (11) due to a static eccentricity of the rotor, a non inertial reference frame $O\xi\eta$ rotating at the angular velocity ω_s can be adopted. The equations of motion are then given by

$$\mathbf{M}^*\ddot{\zeta}_s + \hat{\mathbf{C}}_r^*\dot{\zeta}_s + \hat{\mathbf{K}}_r^*\zeta_s = \mathbf{f}_{rc}\cos\omega_n t + \mathbf{f}_{rs}\sin\omega_n t \tag{15}$$

where $\hat{\mathbf{C}}_r^* = \hat{\mathbf{C}}^* + 2\omega_s\bar{\mathbf{M}}^* - \omega\mathbf{G}^*$ and $\hat{\mathbf{K}}_r^* = \hat{\mathbf{K}}^* - \mathbf{K}_m^* - \omega_s^2\mathbf{M}^* + \omega\omega_s\bar{\mathbf{G}}^* + \omega_s\bar{\mathbf{C}}^*$. The structure of matrices $\bar{\mathbf{M}}^*$, $\bar{\mathbf{G}}^*$, $\bar{\mathbf{C}}^*$ is specified in appendix. In this reference frame the unbalance forces rotate at the angular velocity $\omega_n = \omega - \omega_s$ while the u.m.p. is fixed and can be introduced through the matrix $\mathbf{K}_m^*$. The structure of $\mathbf{K}_m^*$ is the same of $\mathbf{K}^*$ and the non null elements are

$$\begin{aligned}
\mathbf{K}^*_{m11} &= \frac{k_m}{l^2}\left(b^2 + c_p^2\right); \\
\mathbf{K}^*_{m12} &= \frac{k_m}{l^2}\left(ab + c_p\left(a+b\right) - c_p^2\right); \\
\mathbf{K}^*_{m21} &= \frac{k_m}{l^2}\left(ab - c_p\left(a+b\right) - c_p^2\right); \\
\mathbf{K}^*_{m22} &= \frac{k_m}{l^2}\left(a^2 + c_p^2\right)
\end{aligned}$$

where c_p is the distance of the center of the motor from the center of gravity, while a, b are the distances of the sensors of bearing 1 and 2 from the center of gravity and l=$a + b$ (see fig. 1). The displacements at the two planes where sensors are located can be obtained both in the rotating reference frame of equation (15) as $\zeta_s = [\xi_1\ \eta_1\ \xi_2\ \eta_2]^T$ and in the inertial reference frame of equation (12) as $\mathbf{x}_s = [x_{1s}\ y_{1s}\ x_{2s}\ y_{2s}]^T$.

EXPERIMENTAL SETUP

Some preliminary experimental tests have been performed on a prototype of a spindle on active magnetic bearings designed and constructed at the Politecnico di Torino in '90s [7]. The rotor has two radial and one axial magnetic bearings and is equipped by a two poles electric motor. The inertial properties of the rotor are reported in Table (1). The characteristics of the motor and of the PID controller, which is implemented on the whole machine, are respectively indicated in Tables (2) and (3).

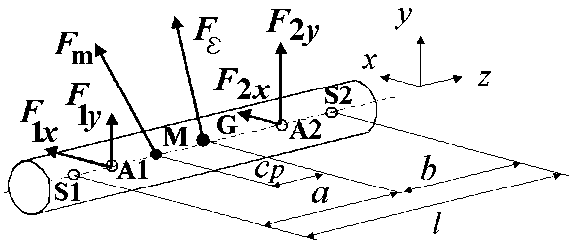

FIGURE 1: Sketch of the rotor on AMBs.

TABLE 1: Inertial properties of the rotor.

Mass	kg	6.13
Mom. of inertia J_t	kgm^2	0.182
Mom. of inertia J_p	kgm^2	0.00277

For the experimental validation of the above model the prototype has been mounted on external supports rotated of 45 degrees about its axis of symmetry. This way it looks isotropic from both the mechanical and the electromechanical points of view, since the bias currents required to compensate for the weight of the rotor are nominally equal along the two axes of the radial bearings. Nevertheless it has been evidenced by spinning the rotor that a slight non isotropy is still present.

TABLE 2: Magnetic suspension data.

Nominal radial gap	mm	0.75
Magnets gain	N^2/A^2	1.672e-6
Control gain K_c	-	1.25
Reset time T_i	s	6.139
Prediction time T_d	s	0.9035e-3
Time constant τ_d	s	50e-6
Sensor gain K_t	V/m	7500
Power Amplifier gain K_a	A/V	1.027

The active magnetic bearings are equipped with a set of five sensors Bently Nevada 3106 mod.20886-01 (eddy currents), that allow the vibration monitoring and the control by measuring the radial and the axial displacements of the rotor along the directions of the active axes of the AMBs. A key-phasor based on a simple OPB701-9708 optical device is installed on the rotor. The current flowing in one phase of the induction motor has been measured by a PR30 Current Probe LEM HEME (maximum current 20 A RMS, output 100 mV/A), while the frequency of this current has been computed by HAMEG HM8122

frequencymeter. The data acquisition is made by Bently Nevada DVF3 Digital Filter, by HP-IB communication system. During the experimental validation the radial displacements (unfiltered and filtered synchronous components) have been acquired, at constant spin speed, startup and shutdown of the machine.

Previous experimental tests identified the unbalance conditions of the rotor written in Table 4, expressed in terms of unbalance components in x and y directions, at the location of the position sensors.

TABLE 3: Induction motor data.

Hanks in parallel	-	2
Turns per phase in series	-	51
Stator winding factor	-	0.85
Rotor diameter	mm	49.5
Stator diameter	mm	51.5
Nominal air gap	mm	1
Motor length	mm	40

TABLE 4: Rotor unbalance components in x and y directions in the planes of the position sensors.

Bearing	axis	[g mm]
1	x	30
1	y	0
2	x	23
2	y	12

EXPERIMENTAL TESTS

Past experiences [10] showed that vibration condition monitoring of the above prototype on AMBs is particularly difficult between few rpm and about 10000 rpm. This range is below the critical speed of first flexural mode of the rotor, while includes two critical speeds of rigid body motion. Since the system is quite highly damped, it is very difficult to define the critical speeds, due to the smoothness of the experimental spin-down curves. Furthermore sensors in x and y directions provide different values of critical speed, due to a residual non isotropy of the system. Four speeds have been identified in spin-down 1850, 2200, 2980, 3200 rpm. A first session of tests has been focused on this spin speed range.

The slip speed at several values of the angular velocity of the shaft has been measured by monitoring the current circulating in one phase of the induction motor at constant spin speed. The maximum and minimum value of the difference between the measured frequencies of the magnetic field and of the shaft are reported in Table (5). At small values of the angular velocity this frequency is quite stable, while at higher values it looks variable in time and

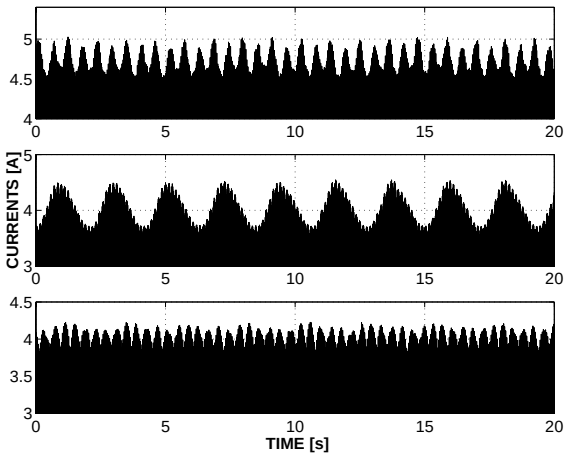

FIGURE 2: Amplitude of the fundamental magnetizing current at 3044, 5930 and 7420 rpm.

affected by higher harmonic contributes as figure (2) shows.

Numerical and experimental results obtained at constant spin speed are compared in figures (3), (4) and (5). A straight line indicates the amplitude peak to peak of the numerical dynamic response of the system considering that both the unbalance and the u.m.p forces act synchronously, without the beat effect. The dotted curve is the amplitude of the experimental value (peak to peak) of the monitored signal, which is compared to the numerical output of the model. A good agreement between numerical and experimental results is obtained by including in the model the ratio (7) proposed by Swann for the computation of the stiffness k_m.

TABLE 5: Experimental slip conditions.

[rpm]	min [Hz]	max [Hz]
2304	0.068	0.068
2414	0.083	0.083
2512	0.082	0.082
3043	0.160	0.160
3538	0.207	0.225
3915	0.267	0.283
4044	0.299	0.312
4205	0.336	0.347
4632	0.411	0.416
5929	0.702	0.714
6614	0.889	0.899
7417	1.123	1.157
8080	1.355	1.375
8317	1.436	1.459
10210	1.859	2.179

At $\omega = 2304$ rpm (figure 3) the rotor is spinning near the first critical speed. The frequency of

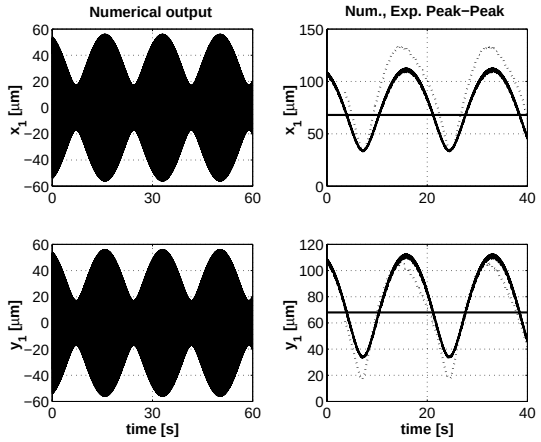

FIGURE 3: Numerical and experimental results at 2304 rpm (bearing 1).

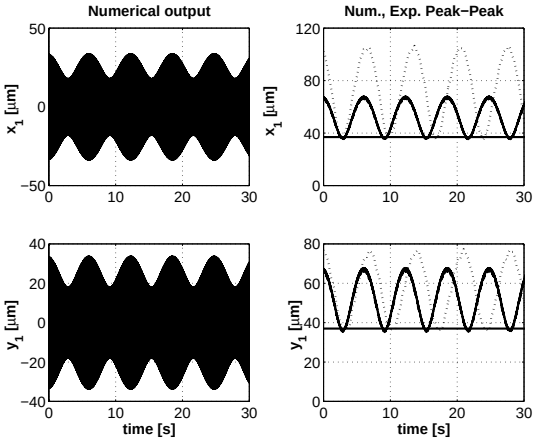

FIGURE 4: Numerical and experimental results at 3044 rpm (bearing 1).

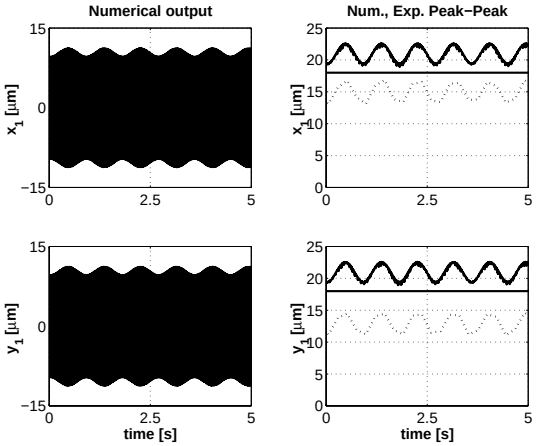

FIGURE 5: Numerical and experimental results at 7417 rpm (bearing 1).

the beat is almost the same for the experimental and numerical outputs, while the amplitude is comparable, altough the experimental signals show a slight residual non isotropy, that the model is unable to predict.

A second test, at $\omega = 3044$ rpm (figure 4), shows the behaviour of the rotor near the second critical speed. There is a small mismatch between the values of the frequency of the numerical and the experimental beats. Actually the slip speed computed by measuring the frequency of the magnetizing current circulating in one phase of the induction motor has been introduced in the model. A good agreement in amplitude is present in the y direction, while x axis is still affected by the already detected non isotropy. Starting from this spin speed the magnetizing current, which flows in the stator winding, looks affected by higher harmonics (figure 2). The motor negative stiffness is consequently not constant in time even if the model assumes the mean value of the magnetising current.

In figure (5) the dynamic behaviour at 7417 rpm is presented. The frequency of the beat is in good agreement with the numerical prediction. The experimental amplitudes are overestimated by the model. This effect was expected according to the experiences reported by Arkkio and Lindgren in [2]. At higher spin speeds it has been observed a reduction of the u.m.p. forces due to the growing eddy currents induced in the rotor conductors, which try to equalise the flux distribution in presence of the rotor eccentricity. U.m.p. looks at least less effective, or in case of very high spin speeds, completely damped [2]. In the present case equalising currents are not enclosed in the analytical model. Actually also in literature the effects of equalising currents, stator and rotor slotting, saturation and unipolar flux are often analysed by time-stepping FEM [4].

VIBRATION MONITORING

The aim of the paper was mainly focused on the vibration monitoring of rotors on AMBs in presence of the u.m.p. effects. The model here proposed looks useful for the analysis of the dynamic behaviour of the rotor within the range of spin speeds where this phenomenon is relevant. In the frequency domain the signals measured by the sensors could show some low frequency harmonics which can be ascribed to the above beat effect. In time domain, models which neglect this phenomenon are unable to predict the large changes in amplitude occurring particularly at lower values of the spin speed, as when performing the preliminary tests of the machine. This problem can be relevant in case of the on-line unbalance detection for balancing [10].

CONCLUSIONS

Vibration condition monitoring of rotors on active magnetic suspension could be significantly affected

by the unbalanced magnetic pull applied by the induction motor in presence of non uniform air gap and slip speed.

In the range of low spin speeds the effect of the u.m.p. could be particularly evident due to a beat occurring between the forces caused by the u.m.p., whose angular velocity is very close to the rotor spin speed, and by the unbalances of the rotor. The amplitude of the radial displacements of the rotor changes at the frequency of the beat, which depends on the occurring slip speed in the induction motor.

At higher values of the angular velocity of the rotor this phenomenon is less appreciated. The eddy currents circulating in the rotor conductors reduce the unbalanced magnetic pull effect on the radial displacements of the shaft. The slip speed increases and the amplitude changes in the monitored positions are smaller. Furthermore selfcentring condition occurring in supercritical regime of the rotor spin speed allows to have smaller dynamic eccentricity.

A dynamic model of the controlled rotor on AMBs including the u.m.p. effect has been proposed and experimentally validated at least in the subcritical regime of the test rotor with respect to the first flexural critical speed of the shaft. A quite good agreement between numerical and experimental results has been found until the values of the spin speed at which other effects, due to the eddy currents and the higher harmonic components of the current flowing in the stator windings, occur.

The above results suggest to include among the signals processed and recorded by the vibration monitoring system some relevant parameters of the induction motor, like the currents circulating in the stator winding, to evaluate these effects on the dynamic behaviour of the controlled rotor on AMBs.

AKNOWLEDGEMENTS

The authors wish to thank for his fruitful support Ing. Enrico Rava of Elettrorava, Savonera, Torino.

APPENDIX

The structure of the matrices $\bar{\mathbf{G}}^*$, $\bar{\mathbf{M}}^*$, $\bar{\mathbf{C}}^*$ used in equation (15) is the following:

$$\bar{\mathbf{G}}^* = \begin{bmatrix} g & 0 & -g & 0 \\ 0 & g & 0 & -g \\ -g & 0 & g & 0 \\ 0 & -g & 0 & g \end{bmatrix} ; \; g = \frac{J_p}{l^2}. \qquad (16)$$

$$\bar{\mathbf{M}}^* = \begin{bmatrix} 0 & -M^*_{11} & 0 & -M^*_{13} \\ M^*_{22} & 0 & M^*_{24} & 0 \\ 0 & -M^*_{13} & 0 & -M^*_{33} \\ M^*_{42} & 0 & M^*_{44} & 0 \end{bmatrix} \qquad (17)$$

$$\bar{\mathbf{C}}^* = \begin{bmatrix} 0 & -C^*_{22} & 0 & -C^*_{24} \\ C^*_{11} & 0 & C^*_{13} & 0 \\ 0 & -C^*_{24} & 0 & -C^*_{44} \\ C^*_{31} & 0 & C^*_{33} & 0 \end{bmatrix} \qquad (18)$$

where all symbols are reported in [10].

REFERENCES

[1] F.M. Abdel-Kader, The characteristic performance of induction motor with eccentricity, Electric Machines and Power Systems, Vol.9, pp.61-70, 1984.

[2] A. Arkkio, O. Lindgren, Unbalanced magnetic pull in high speed induction motor with an eccentric rotor, ICEM 94, Vol. 1, pp. 53-58.

[3] A. Arkkio, Unbalanced magnetic pull in cage induction motors dynamic and static eccentricity, ICEM 96, Vol. 1, pp. 192-197.

[4] D.G. Dorrell, The influence of rotor eccentricity on the output torque of cage induction motors, ICEM 94, Vol. 1, pp. 35-41.

[5] R.L. Stoll, Simple computational model for calculating the unbalanced magnetic pull on a two-pole turbogenerator due to eccentricity, IEE Proc-Electr.Power Appl., Vol.144, N. 4, July 1997.

[6] J.Widmer, G.Genta, P.von Burg, H.K. Asper, Prediction of the dynamic behaviour of a flywheel rotor system by FE-method, Proceedings of the 23rd Intersociety Energy Conversion Engineering Conference, ASME, July 31 - August 5, Denver, Colorado New York, 1988.

[7] C. Delprete, S. Carabelli, G. Genta, Design, Construction, and Testing of a Five Active Axes Magnetic Bearing System, Proc. of 2nd. Int. Symp. on Magnetic Suspension Technology, Seattle, WA, U.S.A., 11-13 August 1993, pp.5.a.21-5.a.35.

[8] P. Hammond, Applied electromagnetism, Pergamon Press, 1971, p.191.

[9] G. Genta, Vibration of Structures and Machines, 3rd ed., Springer, New York, 1998.

[10] E. Brusa, C.Delprete, G.Genta, On line unbalance analysis for monitoring and active balancing of rotors, Proceedings of the Int. Conf. On App. Of Modal Analysis, 15-17 December 1999 Gold Coast, Australia.